Experiments on the Richtmyer-Meshkov Instability II: Nonlinear Evolution of a Shocked Membraneless Single-Mode Sinusoidal Interface

Bhalchandra Puranik, Jason Oakley,
Mark Anderson, Riccardo Bonazza

September 2001

UWFDM-1172

FUSION TECHNOLOGY INSTITUTE

UNIVERSITY OF WISCONSIN

MADISON WISCONSIN

Experiments on the Richtmyer-Meshkov Instability II: Nonlinear Evolution of a Shocked Membraneless Single-Mode Sinusoidal Interface

Bhalchandra Puranik, Jason Oakley,
Mark Anderson, Riccardo Bonazza

Fusion Technology Institute
University of Wisconsin
1500 Engineering Drive
Madison, WI 53706

September 2001

UWFDM-1172

.

Abstract

An experimental investigation of the shock-induced interfacial instability (Richtmyer-Meshkov instability) is undertaken in an effort to study temporal evolution of interfacial perturbations in the nonlinear regime. The experiments are performed in a vertical shock tube with a square cross-section. A membraneless interface is prepared by retracting a sinusoidally shaped metal plate initially separating carbon dioxide from air, with both gases initially at atmospheric pressure. With carbon dioxide above the plate, the Rayleigh-Taylor instability commences as the plate is retracted and the amplitude of the initial sinusoidal perturbation imposed on the interface begins to grow. The interface is accelerated by a strong shock wave (M=3.08) while its shape is still sinusoidal and before the Kelvin-Helmhotz instability distorts it into the well known mushroom-like structures, but its amplitude to wavelength ratio is large enough that the interface evolution enters its nonlinear stage very shortly after shock acceleration. The pre-shock evolution of the interface due to the Rayleigh-Taylor instability and the post-shock evolution of the interface due to the Richtmyer-Meshkov instability are visualized using planar Mie scattering. The pre-shock evolution of the interface is carried out in an independent set of experiments. The initial conditions for the Richtmyer-Meshkov experiment are determined from the pre-shock Rayleigh-Taylor growth. In this article we describe the Richtmyer-Meshkov experiment in detail. One image of the post-shock interface is obtained per experiment and image sequences, showing the post-shock evolution of the interface, are constructed from several experiments. The growth rate of the perturbation amplitude is measured and compared with some of the most recent nonlinear analytical models of the Richtmyer-Meshkov instability.

1 Introduction

The Rayleigh-Taylor (R-T)[1, 2] and Richtmyer-Meshkov (R-M)[3, 4] instabilities occur when two fluids in contact have a relative motion normal to the interface that separates them. The R-T instability results when a light fluid is constantly accelerated into a heavy one; the R-M instability results when an interface is impulsively accelerated by a shock wave passing through it, irrespective of the direction of propagation of the shock wave (and hence of the induced fluid motion). As a result of these instabilities, the amplitude of any perturbations present at the interface grow with time, eventually leading to a fully turbulent mixing of the two fluids. The driving mechanism for these two instabilities is the baroclinic generation of vorticity induced as a result of the non-zero cross product, $\nabla\rho \times \nabla p$, at the interface. For the R-T instability, ∇p is provided by the hydrostatic pressure difference, while in the case of the R-M instability, it is provided by the pressure jump across the shock wave. In both cases, $\nabla\rho$ is the density gradient at the interface.

The R-M instability is a fundamental fluid instability that manifests itself in nature as well as technological applications. In astrophysics, it is used to explain the overturn of the outer portion of the collapsing cores of supernovas and the unexpected mixing in the outer regions of the supernova[5, 6, 7]. It has been used to explain the rapid collapse of gas bubbles in liquids[8, 9] and many other areas yet to be discovered. In technological applications, the R-M instability occurs in inertial confinement fusion (ICF)[10, 11, 12], supersonic and hypersonic combustion in air breathing vehicles[13, 14] and laser-matter interactions[15, 16]. The turbulent mixing induced by the R-M instability is deleterious in ICF applications: the spherical shell that encapsulates the deuterium-tritium fuel becomes R-M unstable as it is accelerated inward by the ablation of its outer surface by laser or secondary X-ray radiation. The mixing between the fuel and the shell material causes dilution of the fuel and limits the compression achieved in these reactions, thus lowering the energy yield. On the other hand, the R-M mixing occurring as a result of the interaction of a shock wave with the flame front can be advantageous in supersonic and hypersonic combustion applications, where rapid mixing of the fuel and oxidizer is desired.

The R-M instability has been studied over the last forty years theoretically, numerically

and experimentally since Richtmyer first presented his linear analysis in 1961. Typically, R-M studies have concentrated in the quantification of the temporal evolution of the amplitude of interfacial perturbations, determination of the growth rates in the linear and nonlinear stages, study of the distortion of the interface into bubbles and spikes and determination of a thickness of the turbulent mixing zone (TMZ) and its temporal evolution. The linear stage of growth of the instability is characterized by the amplitude of a perturbation being much smaller than its wavelength. The growth rate of the instability in this stage can be characterized with Richtmyer's[3] impulsive model:

$$\frac{d\eta}{dt} = k[v]A\eta_0, \tag{1}$$

where k is the wave number of a sinusoidal perturbation (k=$2\pi/\lambda$, λ being the wavelength of the perturbation), η_0 is the initial amplitude, A=$(\rho_2 - \rho_1)/(\rho_1 + \rho_2)$ is the Atwood number (ρ being the density of a fluid and the shock propagating from fluid 1 to fluid 2) and $[v]$ is the velocity jump induced by the shock wave at the interface. However, when the amplitude is no longer small compared to the wavelength the growth becomes nonlinear. The nonlinear effects result in: a decrease in the growth rate, a distortion of the initially sinusoidal interface into shapes referred to as "bubbles" and "spikes", interaction between different modes (in the case of a multimode initial perturbation at the interface) and the onset of secondary Kelvin-Helmholtz instabilities.

Several models have been proposed to describe the growth of the interfacial perturbations in the nonlinear regime. Hecht *et al.*[17] studied the bubble motion in the R-T and R-M instabilities for an interface between an incompressible fluid and a constant supporting pressure, corresponding to an Atwood number of unity. A model was proposed for the bubble motion by considering potential flow near the bubble tips. The model was applied to two-dimensional single mode evolution as well as two-bubble competition. The model predicted that the asymptotic growth rate of a single mode R-M bubble of wavelength λ decays with time as $\lambda/(3\pi t)$, while for the R-T case, it attains a constant asymptotic growth rate, equal to $0.230\sqrt{g\lambda}$. Zhang and Sohn[18] formulated a nonlinear analytic theory to describe all stages of the R-M instability, for the case of a shock wave propagating from a light to a heavy fluid. Their theory is based on the assumption that the R-M unstable system undergoes a tran-

sition from an early linear, compressible stage to a nonlinear, incompressible stage at later times. They developed a general nonlinear perturbative solution for incompressible fluids and evaluated it explicitly for the impulsive model through the fourth order. The early time compressible solution was formulated on the basis of Padé approximations. They matched the two solutions through asymptotic matching. The solutions are found to be:

$$\nu_o = \frac{\nu_{lin}}{1 + \nu_{lin}\eta_0 k^2 t + \max\{0, \eta_0^2 k^2 - A^2 + \frac{1}{2}\}\nu_{lin}^2 k^2 t^2} \tag{2}$$

for the overall growth rate,

$$\nu_b = -\nu_o + \frac{Ak\nu_{lin}^2 t}{1 + 2k^2\eta_0\nu_{lin}t + 4k^2\nu_{lin}^2[\eta_0^2 k^2 + \frac{1}{3}(1 - A^2)]t^2} \tag{3}$$

for the bubble growth rate, and

$$\nu_s = \nu_o + \frac{Ak\nu_{lin}^2 t}{1 + 2k^2\eta_0\nu_{lin}t + 4k^2\nu_{lin}^2[\eta_0^2 k^2 + \frac{1}{3}(1 - A^2)]t^2} \tag{4}$$

for the spike growth rate. Here, ν_{lin} is the growth rate in the linear regime, given by Richtmyer's impulsive model; and post-shock values of A and η_0 are used. It is evident that the following relation exists among these growth rates:

$$\nu_o = \frac{1}{2}(\nu_s - \nu_b) \ . \tag{5}$$

The integration of the above expressions gives the growth of the perturbations. The integration shows that the amplitude growth is predicted to have an inverse tangent dependence on time. Their model predicts that the spike grows faster than the bubble and as the Atwood number decreases, the interface becomes more and more symmetric.

Barenblatt[19] and Mikaelian[20] have proposed analytical models to estimate the thickness of the R-M turbulent mixing zone. Barenblatt's[19] analysis predicts a thickness evolution described by:

$$h \propto t^{\theta}, \tag{6}$$

where t is the time and θ=2/3 without dissipation and $\theta < 2/3$ with dissipation (θ is called the scale invariant R-M parameter). Mikaelian reformulated Read's[21] model for R-T mixing:

$$h = \alpha A g t^2, \tag{7}$$

α is called the scale-invariant R-T parameter and obtained

$$h \propto [v]At, \tag{8}$$

for the R-M case.

Based on the application of potential flow theory at the tips of the bubbles and spikes, Alon *et al.*[22, 23] have proposed the following expressions for the asymptotic growth rates:

$$\nu_b = \frac{C\lambda}{t} \tag{9}$$

where ν_b is the bubble growth rate, C=1/3π for $A \geq 0.5$ and C=1/2π for $A \to 0$ (lower Atwood numbers); and

$$\nu_s = \left(\frac{1+A}{1-A}\right)\frac{C\lambda}{t} \tag{10}$$

where ν_s is the spike growth rate. The amplitude of the perturbations is found by integrating the growth rate which gives a logarithmic behavior in time.

Recently, two new models have been proposed to describe the growth of the R-M instability in the nonlinear regime. Sadot *et al.*[24] proposed a simple formula which fits the linear, early nonlinear and asymptotic behavior of the bubble and spike evolution. This result is a refinement of the formulation proposed by Alon *et al.*[22, 23]. It is expressed in terms of the growth rate, given as:

$$\nu = \nu_0 \frac{1+Bt}{1+Dt+Et^2} \tag{11}$$

where ν_0 is the growth rate in the linear regime, given by Richtmyer's impulsive model and,

$$B = \nu_0 k \tag{12}$$

for the bubble and the spike,

$$D = (1 \pm A)\nu_0 k \tag{13}$$

and,

$$E = \frac{(1 \pm A)}{(1+A)}\frac{1}{2\pi C}\nu_0^2 k^2 \tag{14}$$

where the plus and minus signs are for the bubble and spike respectively. For $A \geq 0.5$, C=1/3π and for $A \to 0$, C=1/2π. Integration of the growth rate expression indicates that the amplitude has a combination of a logarithmic and inverse tangent dependence on time.

The model predictions were compared to numerical simulations as well as experimental data and found to be in good agreement. Ramshaw[25] proposed a model using a Lagrangian energy formulation to describe the bubble growth in the linear as well as nonlinear regimes, for an arbitrary acceleration, g, imposed on a perturbed density interface. The R-T and R-M instabilities were considered special cases of the acceleration. The growth of the bubble amplitude, h, is described in terms of the differential equation

$$bh\ddot{h} + \frac{bh}{2h}\dot{h}^2 + 2\pi c\dot{h}^2 - 2\pi Agh = 0 \tag{15}$$

where b is a model constant and c is a dissipation factor (b and c are expressed in terms of the scale-invariant R-T parameter, α, and the R-M power law exponent, θ; both α and θ are chosen from previous experimental results.) Therefore, the model is semi-empirical. If the R-M case is considered to have no acceleration for $t > 0$, the final term in the above equation can be dropped for late time growth. The equation can then be rearranged in the following form:

$$h\ddot{h} + \left(\frac{1}{2} + \frac{2\pi c}{b}\right)\dot{h}^2 = 0 \ . \tag{16}$$

This equation can be solved with the following result:

$$h = h_1\left[1 + p\left(\frac{\dot{h_1}}{h_1}\right)(t - t_1)\right]^{1/p} , \tag{17}$$

where h_1 and $\dot{h_1}$ are the values at $t = t_1$, and

$$p = \frac{3}{2} + \frac{2\pi c}{b} \ . \tag{18}$$

The constant, p, is related to the R-M power law exponent, θ by:

$$\theta = \frac{1}{p} \ . \tag{19}$$

Most of the past experimental investigations of the R-M instability have been carried out in shock tubes where results have been limited to weak shocks to keep the pressure loads within the structural limits of the existing facilities. The behavior of the instability for moderate to strong shocks remains to be investigated. Many shock tube investigations in the past[4, 26, 27, 28] have used thin nitrocellulose or mylar membranes (about 1 μm thick) to separate the two gases initially to form an interface. These membranes are, in general,

undesirable in order to study the behavior of the instability in its purest form. A survey of previous investigations shows that experimental data are needed in the nonlinear regime of growth of the interfacial perturbations for providing a set of benchmarking data for the analytical models and numerical calculations being developed worldwide. Thus, the two primary goals of the present work are: 1) to perform R-M instability experiments with strong shocks ($M \geq 2$) in a large cross-section shock tube (in order to eliminate any wall effects on the growth of the perturbations), and 2) to perform planar imaging of the R-M unstable interface and measure growth rates of the perturbation amplitudes in the nonlinear stages of evolution. In order to create a membraneless interface between the two gases, we utilize the retractable plate technique described in part I of this two part series by Puranik *et al.*[29]

2 Experimental setup

2.1 Wisconsin Shock Tube and related instrumentation

The experiments are performed in the Wisconsin Shock Tube[30]. The shock tube has several key features: 1) a large internal square cross section (25×25 cm^2) for minimizing wall boundary layer effects, 2) a vertical orientation for preparing a gravitationally stratified interface between two gases, 3) a strong structural capacity for studying strong shock waves in gases at atmospheric pressure (maximum design pressure is 10 MPa), 4) a modular construction for studying interfaces of different ages and 5) a boost tank for rupturing the diaphragm at a precise time. The shock tube is equipped with an interface section and a test section. The interface section, located above the test section, has slots where an interface between two gases may be formed using a thin membrane or a retractable plate. Flow visualization takes place in the test section where optical access is available through a 24 cm diameter fused quartz window. An interface may also be formed in the test section by retracting a plate out of the test section through the plug on the opposite side from the window.

A Continuum (Surelite II-PIV) pulsed Nd:YAG laser is used as the light source for imaging. The laser consists of two laser cavities capable of delivering 200 mJ/pulse (and hence

400 mJ/pulse when the beams are superimposed) at a wavelength λ=532 nm, with a pulse width of 10 ns. A CCD camera (Spectra Video Series, by Pixel Vision) is used to capture the post-shock flowfield images. It has a backlit, thermoelectrically cooled, 1024×1024 pixel array, with a 16 bit resolution per pixel. The camera is controlled with a personal computer which also stores the image. An 105 mm f2.8, focal length AF Nikkor Micro lens is used with the camera. In order to visualize the post-shocked interface, a planar Mie scattering technique is employed. The test gas is seeded with filtered cigarette smoke with an average particle size of less than 0.5 μm[31]. The degree to which the smoke particles track the flow has not been quantified, however, based on particles of similar size[32], the smoke particles are believed to closely track the flow velocity for the velocities and time-scales of the experiment. For further detail the reader is referred to part I of this two part series[29].

2.2 Experimental procedure

At the time of an experiment, the entire optical setup and a portion of the shock tube containing the test section are surrounded by an enclosure made of thick theater curtains so the area surrounding the test section is completely dark. Wall-mounted piezoelectric pressure transducers are used in the driven section of the shock tube to measure the incident shock speed, and to trigger the laser to pulse (through a variable delay box).

First, the driven section is evacuated to approximately 6 kPa and filled with driven gas to atmospheric pressure. This procedure is repeated twice to achieve the desired gas purity. The supply of the driven gas is continued until approximately two volumes of the driven section have been flushed. The sinusoidal retractable plate and its support frame are inserted in the interface section. At this time, driven gas is present above and below the plate. Now, the driver section is evacuated to about 2 kPa and filled with the driver gas to just above atmospheric pressure. The test gas is slowly introduced into the portion of the driven section below the interface plate to minimize any leaks past the retractable plate into the portion above it. The test gas enters from the bottom flange of the shock tube and displaces the driven gas upward. This driven gas exits the shock tube just below the plate. After approximately two test section volumes worth of test gas is circulated, the direction of the flow is reversed. Now, the test gas is introduced just below the plate and flows downward

to exit from the end wall of the shock tube until two more volumes are circulated and the filling is stopped. This minimizes contamination of the test gas by the driven gas. The purity of the gases is confirmed by the fact that the transmitted shock speed (for a given incident shock speed) is within 1% of the value predicted by one-dimensional gas dynamics calculations.

The driver section is then pressurized with the driver gas to a pressure about 200 kPa below the predetermined diaphragm rupture pressure (which is known from the diaphragm characterization). The 0.15 m^3 boost tank is pressurized to 15 MPa. The laser flashlamp capacitor is charged and a reed switch is opened which enables the laser to remain charged. Oscilloscopes are set to record the pressure transducer signals. The camera shutter is opened and the CCD exposure is set for 6 seconds. The plate retraction is started using a pneumatic mechanism. The voltage output from a linear voltage displacement transducer (LVDT) attached to the retractable plate begins to change as the plate starts retracting. A trigger signal is sent electronically (using the LVDT signal and a solid state relay) to the boost tank valve after the plate has traveled a predetermined distance. The boost tank overpressurizes the driver section rapidly until the diaphragm is ruptured. By the time the shock wave arrives at the interface location, the plate has retracted out of the interface section completely and a mechanical gate seals off the opening through which the plate slides out. The shock wave is sensed by the wall-mounted pressure transducers. The signal from a wall mounted pressure transducer is used to shut off the boost tank and to trigger the laser to pulse.

The retraction of the plate is performed in two stages. Figure 1 shows the schematic of this process. The laser sheet is projected approximately at the center of the shock tube. The plate is retracted slowly until it crosses the plane of the laser sheet. This is done to minimize any disturbances the plate may introduce in the gases at the interface. This first stage is carried out in approximately 250 ms and is represented in the schematic by τ_1. At this instant, the two gases come in contact with each other in the plane of the laser sheet and the R-T instability begins to develop. The plate is then retracted out of the interface section rapidly (in approximately 70-80 ms) by providing a pressure boost to the pneumatic piston. This process is represented by τ_2 on the schematic. The objective is to have the plate retracted out completely by the time the shock wave arrives at the interface. Furthermore,

it is undesirable to have the R-T instability evolve to a point where the K-H instability generates vortex roll-ups. The LVDT attached to the retractable plate is used to provide the signal for the pressure boost to the pneumatic piston as well as to trigger the boost tank to rupture the diaphragm. The diaphragm rupture time is estimated to be 180 ms after the trigger signal is sent to the boost tank. The LVDT signal corresponding to the plate edge being at the laser sheet location is noted before the experiment. Thus, the time at which the edge of the retractable plate crosses the laser sheet location is known and the age of the R-T developed interface at the arrival of the shock can be estimated readily. The inherent uncertainty in the rupture process of the diaphragm, however, results in an interaction of the incident shock wave with an interface having a different initial amplitude determined by the R-T instability growth, each time the shock is fired. Note that we currently can obtain only one image per rupture of the diaphragm. Therefore, an experimental database consisting of different initial interfaces, accelerated by a Mach 3.08 shock wave incident in CO_2, is generated. Due to careful characterization of the diaphragm rupture, we are able to accelerate an initial interface that has a R-T age of 110 ms.

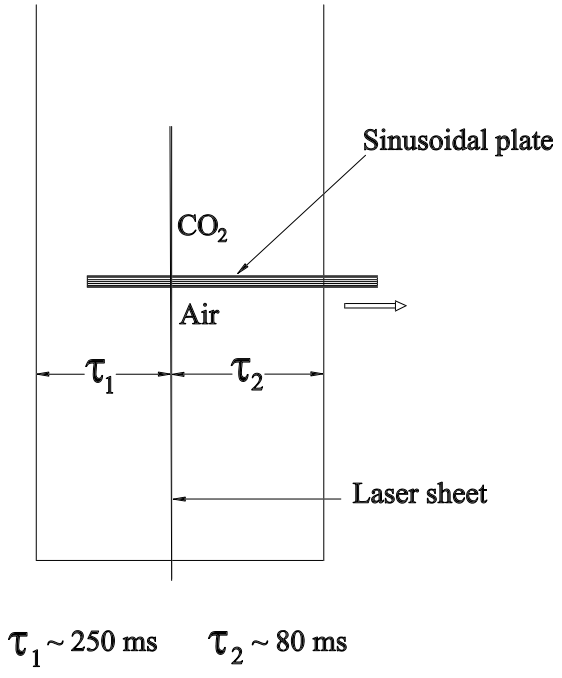

Figure 1: Schematic showing the two-stage retraction process for the sinusoidal plate.

Table 1: List of relevant physical parameters for a M=3.08 shock wave incident on a CO_2-air interface.

M	W_{i} (m/s)	$[v]$ (m/s)	ρ_{CO_2} (kg/m^3)	ρ_{air} (kg/m^3)	A	ρ'_{CO_2} (kg/m^3)	ρ'_{air} (kg/m^3)	A'
3.08	830.2	699.1	1.799	1.184	0.206	7.158	4.307	0.249

3 Experimental results

To study the temporal evolution of the R-M instability, the interface section is placed at different distances from the test section by reconfiguring the shock tube. The distance between the center of the test section window and the initial interface location is increased through the following values: 0.452 m, 0.757 m, 0.957 m, 1.261 m and 1.465 m. Corresponding to these distances, the ages of the shock-accelerated interface are: 646 μs, 1.083 ms, 1.368 ms, 1.804 ms and 2.095 ms respectively. In addition to these relative positions, the interface is formed in the test section itself for some experiments, to visualize the very early interaction of the shock wave with the interface. For this purpose, the window plug in the test section is modified to accommodate the retractable plate. Thus, the test section may also perform as an interface section.

The relevant physical parameters are listed in Table 1. Note that CO_2 and air are initially at atmospheric pressure and room temperature. Furthermore, the initial amplitude, η_0, is different every time the shock is fired. In the table, W_{i} is the incident shock wave velocity, $[v]$ is the velocity of the interface and primed quantities denote post-shock values calculated from the solution to the corresponding 1-D Riemann problem.

3.1 Visualization results

In this section, example experimental images of the R-M unstable interface are presented. All images shown are contrast-enhanced, raw experimental data. In all images, the incident shock wave travels from the top (CO_2) to the bottom (air seeded with smoke).

3.1.1 Phase inversion

A shock-interface interaction, with the shock traveling from the heavy to the light gas, results in a phase inversion of the initial sinusoidal perturbations[4]. The perturbations continue growing in time thereafter, maintaining the changed phase. The phase inversion phenomenon is not observed in the case of a shock traveling from the light to the heavy gas. These phenomena can be explained on the basis of vorticity generation at the interface by baroclinic processes. It can be recalled that the driving mechanism for the R-M instability is the baroclinic generation of vorticity induced as a result of the non-zero cross product, $\nabla\rho \times \nabla p$, at the interface. Figure 2 shows the vorticity generation at the interface during a shock-interface interaction. It may be pointed out that the vorticity is deposited at the interface only during the time it takes for a pressure equality to establish between the reflected shock wave and the transmitted shock wave (in the case of the incident shock wave traveling from light to heavy fluid) or between the reflected expansion wave and the transmitted shock wave (in the case of the incident shock wave traveling from heavy to light fluid). The perturbation growth is caused by the dynamic evolution of the deposited vorticity at later times. From Fig. 2, it is clear that the sense of vorticity (clockwise or counterclockwise) depends upon the direction of shock propagation, and how it causes a phase inversion for the heavy/light configuration.

Figures 3 (a)-(d) show a few typical images obtained when the interface is initially in the center of the test section window. Figure 3(a) shows a pre-shocked initial interface. The incident shock wave is yet to accelerate it. The edge of the retractable plate is seen as the thin bright sinusoidal line above the contour of the interface. The laser sheet is 0.3 mm thick, and Mie scattering in the test gas (air) in the bottom half of the image, shows an expanding fan of light from the bottom, to a width of 11.5 cm at the interface. The Mie scattering signal is not a uniform value across the width of the laser sheet due to variations in the laser beam and is typically brighter in the middle of the sheet and weaker at the sides of the sheet. There are also variations in the laser beam from pulse to pulse which results in the Mie scattering signal differing from experiment to experiment. The formation of the sinusoidal R-T-developed interface is clearly seen in this image. Note the phase of the

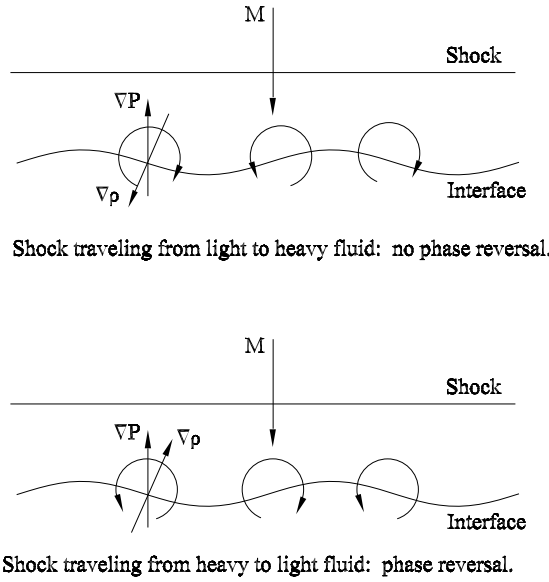

Figure 2: Schematic showing the shock-interface interaction for the case of a shock traveling from a light to a heavy gas and vice versa, illustrating whether or not the deposition of vorticity results in phase reversal.

sinusoidal interface being formed. Figure 3(b) shows the progress of the incident shock wave through the interface. Note that the shock wave is visualized as the bright horizontal line seen approximately halfway through the interface. The number density of smoke particles is increased enormously in proximity of the shock wave, thus increasing the scattering signal. It can be readily seen that the shock wave has compressed the initial interface. The initial crest locations are seen flattening behind the shock. The interface is not completely flattened yet: a slight convexity of the crests is still observed.

Figure 3(c) shows an image captured slightly later in time, with the transmitted shock further into the light gas. The flattening of the initial crests is seen to be almost complete. This image shows the early stages of the phase inversion process and an incipience of troughs in the original crest locations is clearly evident. The transmitted shock is clearly seen to have a sinusoidal shape, with its crests and troughs in the same locations as the crests and troughs of the original sinusoidal interface, respectively. Figure 3(d) shows the conclusion of the phase reversal process. From this image, the emergence of a crest at an original trough and the emergence of a trough at an original crest is clearly seen. The phase reversal process

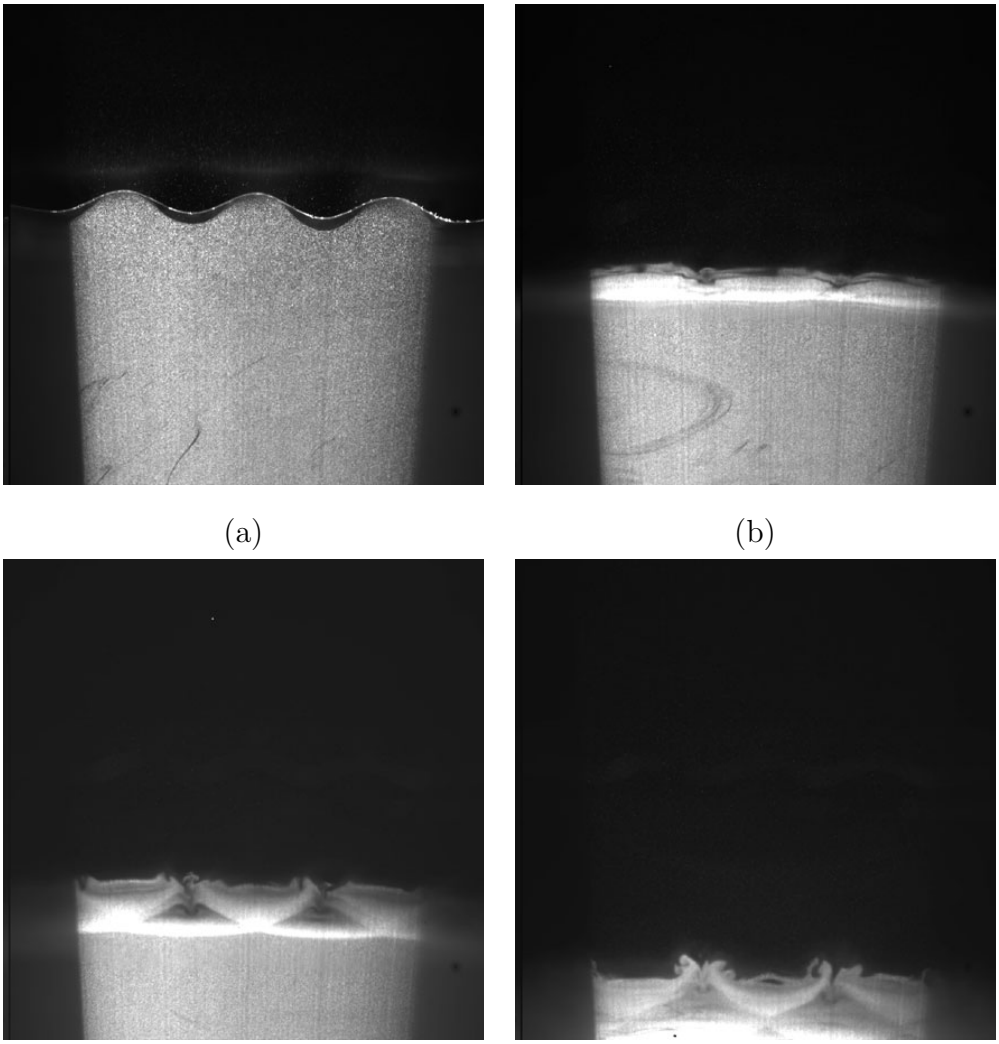

(a) (b)

(c) (d)

Figure 3: Images showing the very early interaction of the shock wave with the interface. (a): pre-shocked initial interface (t=0 s); (b): compression of the initial interface by the shock wave (t=5 μs); (c): progress of the shock wave through the interface leading to the phase reversal of the original sinusoidal perturbations (t=36 μs); (d): final stage of the phase reversal (t=39 μs).

is estimated to take approximately 40 μs after the initial shock contact with the crests of the interface.

There are two types of phase inversions possible during a shock-interface interaction: direct and indirect[33]. The direct phase inversion occurs at or before the conclusion of the shock-interface interaction while the indirect phase inversion occurs as a result of the shock-

interface interaction, during the later dynamical evolution. It is believed that the direct phase inversion occurs only when the incident shock (and hence the reflected rarefaction off the interface) is sufficiently strong. In general, an indirect phase reversal is to be expected. The phase inversion observed in our experiments seems to fall into the latter category.

3.1.2 Temporal evolution of phase inverted interfacial perturbations

Figures 4 (a)-(d) show images of the shocked interface at 646 μs, 1.08 ms, 1.80 ms and 2.10 ms respectively, after the initial shock acceleration. All images show post-shock interfaces that are in the nonlinear stages of growth and clearly not sinusoidal. The smoke particles have been shown to be following the flow, since the interface location is very close to that predicted by one-dimensional gas dynamics. The phase inversion is clearly seen in these images, with presence of troughs in places of original crests and vice versa. The growth of all crests/troughs is not seen to be identical. This is in general observed in all experimental images. We believe that part of the reason for this is the fact that the crests/troughs in the initial R-T unstable phase do not grow by identical amounts. Due to imperfections in the profile on the retractable plate and minute changes in the plate retraction each time, it is observed that the R-T instability does not grow all crests/troughs identically. Moreover, if the incident shock is not exactly planar, it does not come in contact with the sinusoidal interface at once. The shock-induced flow is approximately two orders of magnitude faster than that in the pre-shock R-T case. Any small irregularities on the initial R-T developed interface (which constitute higher order modes) grow rapidly after the initial shock acceleration. This, coupled with the phase inversion process, seems to result in additional turbulence making the post-shock interfacial contour deviate from being smooth and sharply defined. The crests and troughs seem to grow sideways after the phase reversal; this is more apparent in late time behavior (Figure 4 (c)). The reason for this is probably some lateral growth of skewed initial perturbations, especially during the dynamical evolution in the late stages. This observation shows that the late stages of the R-M instability are extremely sensitive to the initial conditions. In the highly nonlinear stages of growth, there is considerable interaction between adjacent mushrooms and an incipience of turbulent mixing can be identified. Furthermore, the mutual penetration of the two gases slows down considerably and an increase in lateral movement

of the mushrooms is observed. The instability growth at this very late time results in a mixing zone (Figure 4 (d)). The interfacial contour is no longer discernible. CO_2 penetrates into the air and as a result of lateral mixing, a cloudlike region is generated. At this point, it is difficult to determine the extent of the penetration of CO_2 into air, due to a lack of measurable difference in the scattering signal obtained off the smoke particles entrained in the mixing region from that obtained off the smoke particles in the pure air region away from the mixing zone. Since the intensity of the laser light in the sheet is not uniform across the width and since due to the shot-to-shot variations, the peak of light intensity is seen to shift from the center of the sheet toward its edges, the identification of the penetration of CO_2 into air is difficult, as it is uncertain if an apparent weakness of the scattering signal is due to the presence of CO_2 or an inherent decrease of intensity in the sheet. In such late stages of the instability, when mixing of the two gases needs to be studied, a technique such as Rayleigh scattering would be useful along with a laser with minimal shot to shot variation. In such a case, a signal calibration would help identify the pure gases from the mixing zone.

3.2 Image processing

The instability growth is described in terms of the peak-to-peak amplitude, measured from the experimental images. An image processing algorithm is adopted for this purpose. The camera used to capture the R-M images has a 1024×1024 pixel array, with a 16 bit resolution per pixel; the typical range of pixel values in the experimental images is 1700-6500 out of a possible 65536. Figure 5 shows an image enhanced so that the pixel values fall within the range of two standard deviations from the average of the pixel values. The image shows a CO_2-air interface, accelerated by a Mach 3.08 shock wave, 646 μs after the shock interaction. The instability growth is seen clearly in this image; however, the image is not very "clean". In particular, there are a number of high intensity specks present in the portion above the interfacial contour and the intensity in the laser sheet is not uniform across the width. The high intensity specks present in the otherwise dark portion of the image constitute an "outlier" type of noise. To remove it, a nonlinear spatial filter based on order statistics is applied. In particular, considering the type of noise and the fact that we are interested in determining the contour of the interface, a median filter with a filter mask of appropriate

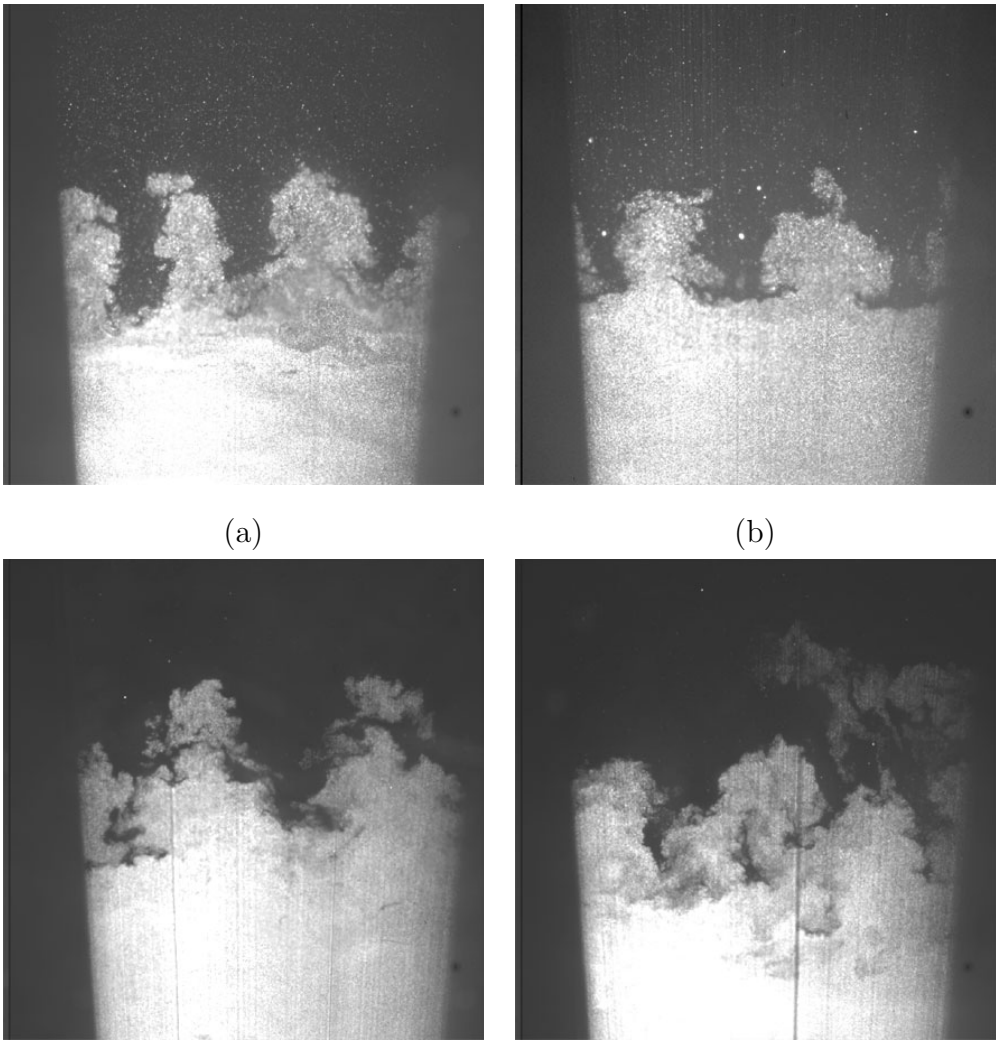

Figure 4: Images showing the late time evolution of the interface following the phase reversal. Images (a)-(d) are captured at 646 μs, 1.08 ms, 1.80 ms and 2.10 ms respectively, after the initial shock acceleration. Development of a mixing zone is evident by the latest stages of the evolution.

order is employed. The median filter is shown to perform well to remove outlier type of noise while preserving edges in an image[34], in that blurring of the image, associated with the application of a low-pass filter, is minimized. The order of the filter mask is determined as the minimum order of the mask that removes the noise. In a filter mask F of order N, a set of $(N-1)$ pixels surrounding a given pixel are considered. The pixels are ordered from

their minimum values to maximum values as follows:

$$F_{(0)} \leq F_{(1)} \leq \cdots \leq F_{(N-2)} \leq F_{(N-1)}, \tag{20}$$

where $F_{(0)}$ and $F_{(N-1)}$ are the minimum and maximum values of the pixels considered in the mask, respectively. The median filter is then defined as:

$$F_{med} = \begin{cases} \frac{F_{(N/2)}+F_{(N/2-1)}}{2} & \text{if } N \text{ is even} \\ F_{((N-1)/2)} & \text{if } N \text{ is odd .} \end{cases} \tag{21}$$

After the high frequency noise is removed from an image, the pixel values above the average pixel value of the image are set to the maximum pixel value of the image and those below the average pixel value are set to the minimum pixel value of the image. This procedure makes the intensity of scattering signal uniform across the width of the sheet and divides the image portions separated by the interface contour into two distinct regions of uniform intensities, while maintaining the shape of the interface contour intact. Figure 6(a) shows the result of this operation. Finally, a contour finding routine is employed on the "cleaned" image to extract the shape of the interfacial contour. Figure 6(b) shows the extracted contour from the cleaned image. The peak-to-peak amplitude is then measured, as an average of the minimum and maximum mutual penetrations by the two gases. These are shown in Fig. 6(b) as η_1 and η_2, respectively. The average peak-to-peak amplitude is denoted by η and represents the overall growth of the instability. A growth factor, F, is then defined as the ratio of the average peak-to-peak amplitude of the shocked interface to that of the corresponding initial interface.

4 Experimental growth rates compared with recent nonlinear models

In this section, the experimentally measured growth of the R-M instability is compared with the predictions from existing nonlinear theories. As mentioned earlier, by careful characterization of the diaphragm rupture, we have been able to accelerate an initial interface that is approximately 110 ms R-T old. At this stage, the initial interface is sinusoidal with an

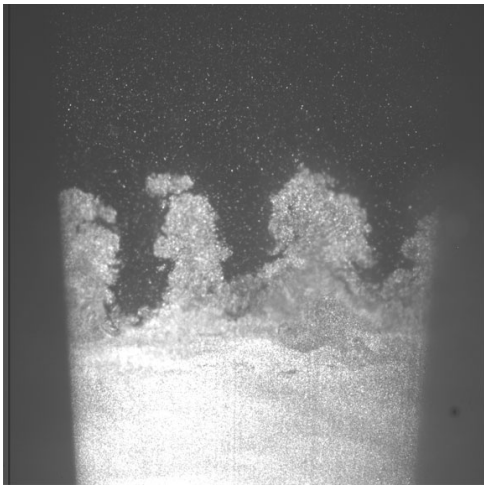

Figure 5: Example of a R-M experimental image, enhanced in contrast.

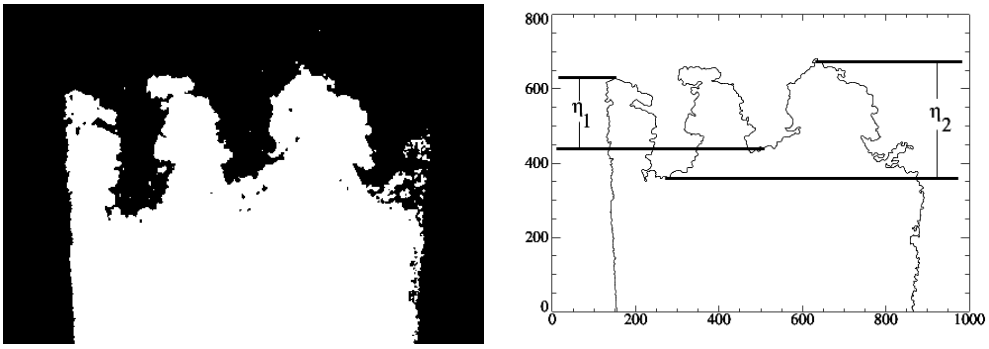

(a) (b)

Figure 6: Processed image (a) result of spatial filtering and adjusting the uniformity of the scattering signals; (b) shows the extracted interface contour with the minimum and maximum mutual penetrations by the two gases.

amplitude to wavelength ratio of 0.232. Therefore, the initial perturbation is considerably nonlinear. Table 2 lists the following:

- The distance, X, between the centers of the test section and the interface section.
- The post-shock delay time corresponding to the X (the age of the R-M imaged interface). There are multiple values for the amplitude at each post-shock delay time because each experiment had a different pre-shock amplitude. The differing preshock

amplitudes correspond to different ages of the R-T interface when it was shocked.

- The initial (pre-shock) peak-to-peak amplitude
- The measured peak-to-peak amplitude at the given post-shock delay corresponding to X.

The theoretical peak-to-peak amplitude at any time is found by integrating the growth rates for the spike and bubble separately and adding the results. In all theories, the post-shock values of the initial amplitudes are used along with the post-shock value of the Atwood number. Furthermore, the phase inversion observed in the experiments is ignored in the calculation. The post-shock value of the initial amplitude is determined using the relation suggested by Richtmyer:

$$\eta_0^{'} = \eta_0 \left(1 - \frac{[v]}{W_{\mathrm{i}}}\right), \tag{22}$$

where $[v]$ is the mean velocity of the interface and W_{i} is the velocity of the incident shock. Substituting the values for the velocities of the incident shock and the interface, it can be seen that the post-shock amplitude is approximately 15.8% of the pre-shock amplitude, indicating the compression associated with a strong shock wave.

In order to compare with the predictions from the various theories outlined in the introduction, all data points with a peak-to-peak amplitude of the initial (preshock) perturbation within a range of 14.39 mm to 20.96 mm are selected. Considering the fact that the pre-shock initial amplitude is compressed to approximately 15.8%, the corresponding post-shock initial amplitudes fall within ± 0.5 mm of an average value of 2.79 mm. This average value is used as the initial amplitude for all theories.

Figure 7 compares the experimentally measured peak-to-peak amplitude with the theoretical prediction. It can be seen that there is a qualitative agreement between the experimental data and predictions from nonlinear theories. The impulsive model overpredicts the growth at all times, as expected. Recall that Alon *et al.*[22, 23] theory predicts the asymptotic growth of the perturbations. Hence, it is plotted for moderate to late times only. The experimental data falls between the predictions from the Sadot *et al.*[24] theory and the Zhang and Sohn[18] theory. At late times, the slope of the Sadot *et al.*[24] curve and the Alon *et al.*[22, 23] curve are similar. The Zhang and Sohn[18] theory underpredicts the perturbations growth at all

Table 2: Experimentally measured peak-to-peak amplitudes (η) and corresponding initial pre-shock peak-to-peak amplitudes (η_0).

X (m)	t (ms)	η_0 (mm)	η (mm)
0.452	0.646	12.52	24.69
		17.67	34.24
		17.16	27.21
		16.64	31.47
		9.10	34.78
		9.82	26.29
0.757	1.083	28.94	34.88
		20.96	51.07
		18.25	31.37
		10.79	31.93
0.957	1.368	16.64	36.24
		17.67	34.10
		16.64	29.32
		20.44	46.47
1.261	1.804	18.25	45.78
		18.84	41.15
		18.25	33.72
		19.64	36.50
		15.57	43.43
1.465	2.095	18.25	45.54
		17.67	31.86
		14.39	36.23

times and predicts saturation at very early times. The prediction from Sadot *et al.*[24] theory agrees best with the data. The theories have been reported to agree well with experiments involving weak shocks (on the order of 1.5). The incident shock in the present experimental campaign is considerably strong, which could have a significant influence on the behavior of the instability. Furthermore, the initial growth rates in Zhang and Sohn[18] theory and the Sadot *et al.*[24] theory are approximated by the value obtained using Richtmyer's impulsive model. However, it should be noted that the behavior of the impulsive model for strong shocks and highly nonlinear initial perturbation is doubtful.

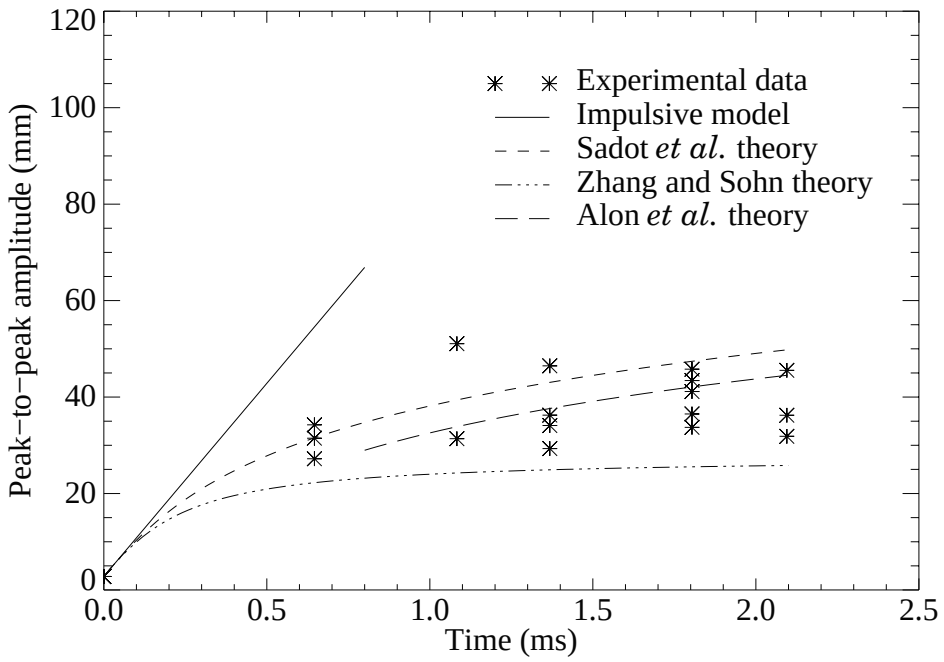

Figure 7: Comparison of the experimentally measured instability growth with predictions from nonlinear theories. The prediction from the impulsive model is shown for qualitative comparison.

Figure 8 shows the prediction of the Ramshaw[25] model compared with the experimental data. The experimental data seem to fall between the predictions using p=1.923 and p=1.492. The reciprocal of the constant p is equal to the scale invariant θ parameter, proposed for the R-M mixing zone growth[25]. Thus, the experimental data yields a value of θ=0.595$\pm$0.075, which is consistent with $\theta \leq 2/3$ where 2/3 corresponds to the zero dissipation case from elementary scaling arguments[25].

5 Influence of initial nonlinearity

At a given configuration of the shock tube, the distance between the test section and the interface section is fixed and so is the post-shock delay time of capturing an image. In an effort to qualitatively study the effect of initial nonlinearity of the interface on the post-shock growth, experiments are carried out to accelerate the initial R-T developed interface

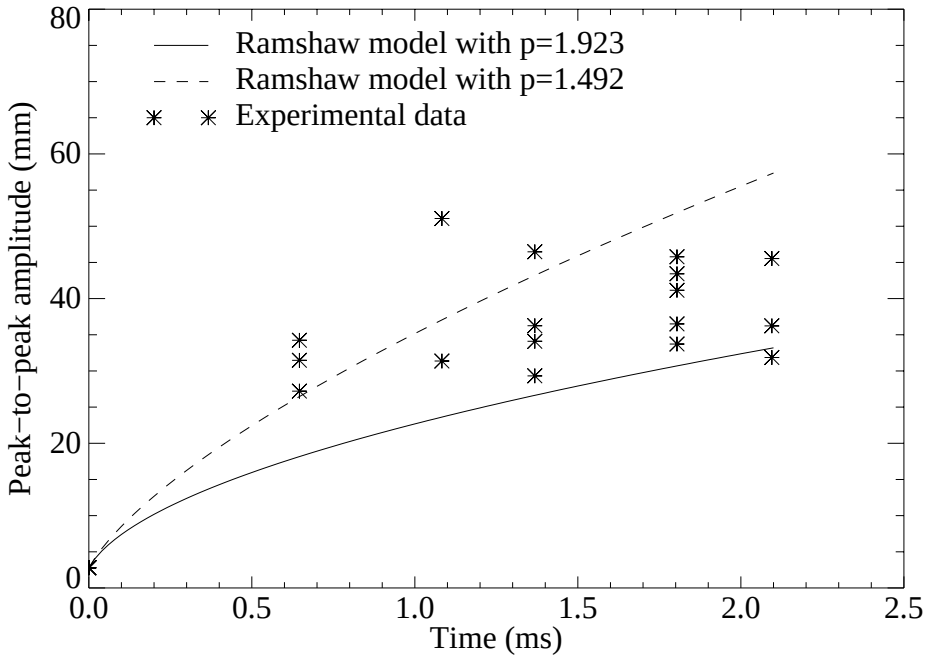

Figure 8: Comparison of the experimentally measured instability growth with prediction from the Ramshaw[25] model.

at different stages of its growth. In order to achieve this, the instant at which the trigger signal is sent to the boost tank to rupture the diaphragm is either advanced or delayed. The plate retraction is nominally identical in each case.

A dimensionless parameter τ_{rt} is formed as the ratio of the absolute age of the initial R-T-developed interface to a characteristic Rayleigh-Taylor time defined by

$$\tau_{rt,c} = \frac{1}{\sqrt{kgA}} \ . \tag{23}$$

Therefore, τ_{rt} describes the nonlinearity of the initial R-T-developed interface: the higher the value of τ_{rt}, the more nonlinear the initial interface is. A second dimensionless parameter τ_{rm} is formed as the ratio of the absolute age of the shocked interface to a characteristic Richtmyer-Meshkov time defined by

$$\tau_{rm,c} = \frac{1}{k[v]A'}, \tag{24}$$

where $[v]$ is the velocity of the accelerated interface. Thus, τ_{rm} is a measure of the nonlinearity

of the shocked interface. A dimensionless nonlinearity ratio, R, is defined as follows:

$$R \equiv \frac{\tau_{rm}}{\tau_{rt}} \ . \tag{25}$$

Thus, low to moderate values of R imply that the initial interface is highly to moderately nonlinear and moderate to high values of R imply that the initial interface is moderately to marginally nonlinear. The growth of the perturbation is measured as the ratio of the peak-to-peak amplitude at any time to the initial peak-to-peak amplitude. Thus, a growth factor is defined as:

$$F \equiv \frac{\eta}{\eta_0} \ . \tag{26}$$

In the above definition, the pre-shocked initial amplitude is used, without loss of generality. Figure 9 shows the growth factor (F) for different nonlinearity ratios (R). Qualitatively, it can be said that the growth factor increases as the initial nonlinearity factor increases. In other words, the more nonlinear the initial interface is, the sooner its growth saturates. The interaction between adjacent mushroom structures that dominates the mixing in late stages occurs sooner for an initial interface with low R. On the other hand, mushroom structures resulting from an interface with high initial R continue to grow independently for a longer period of time. It must be pointed out that several initial R-T-developed interfaces in this campaign are in a highly nonlinear stage and are no longer sinusoidal.

6 Issues concerning present technique

In this section, a few important points regarding the retractable plate technique and the optical diagnostic technique are outlined. The plate retraction technique developed during this experimental campaign is suitable only for the heavy/light configuration. It was shown in part I[29] that with the light/heavy configuration, the interfacial perturbations flatten out due to dispersion of the stable Rayleigh-Taylor oscillations and any discernible perturbations have a very small amplitude after very short times. The heavy/light configuration provides a sharp, single mode nonlinear interface as an initial condition for the R-M experiment. It may be noted that such an initial interface is not stationary, but the perturbations are growing due to the R-T instability. Therefore, in reality, the initial conditions consist of an amplitude

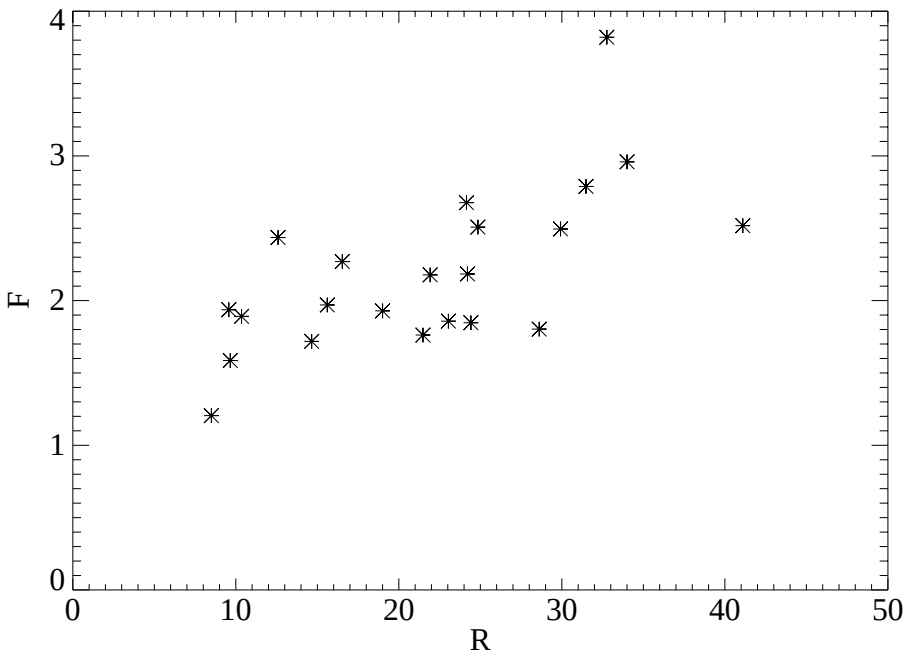

Figure 9: Growth factors for different initial conditions with decreasing nonlinearity.

and a finite growth rate. The presence of an initial growth rate is ignored while comparing experimental data with theoretical predictions, which assume a stationary initial amplitude. However, we also note that the initial velocity is negligible compared to the shock induced velocity.

The retraction of the plate initially separating the two gases induces three-dimensional effects in at least two ways. First, the plate leaves behind it a wake and a small amount of fluid is dragged with the plate that bounces back off the shock tube walls in the form of a gravity wave. In all images obtained during the experiments these effects are not explicitly observed and the flowfields seem predominantly two-dimensional. However, these effects are present and probably affect the instability behavior. Second, as the plate begins to retract, the two gases come in contact in the region between the wall of the shock tube containing the test section window and the edge of the plate and the R-T instability begins to develop immediately. This is exaggerated and schematically shown in Fig. 10. The instability begins to grow in the region S, but the plate has not passed the plane of the laser sheet yet. Thus, the incident shock does not "see" a level interface. Rather, the shock impinges on

region S gradually, resulting in extremely complicated shock diffractions and reflections off the envelope that bounds S and inducing three-dimensional effects in the flowfield. This phenomenon is not accounted for while comparing our experimental results with theoretical predictions.

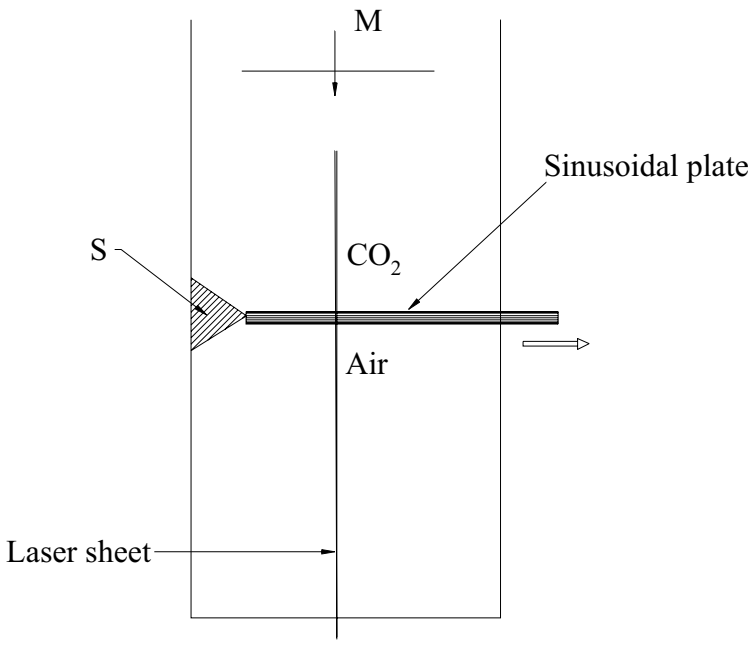

Figure 10: Schematic description of the physical processes responsible for introducing three-dimensional effects.

During the experimental campaign, the formation of consistent initial conditions is observed for approximately 80% of the time. Figure 11 shows images from two different experiments. The images show two interfaces 1.26 ms after initial shock acceleration. From the oscilloscope traces, the initial conditions are expected to be nominally identical; however the shock accelerated interfaces are completely different. Figure 11(a) is close to the expected result, with the presence of distinct peaks and troughs while Fig. 11(b) is far from the expected result. Figure 11(b) is a useful data point only if the initial condition corresponding to it is explicitly known. Therefore, it is concluded that it is essential to image the initial conditions dynamically during the experiment. The interface section of the shock tube has been modified to make it possible to image the pre-shock R-T development and capture

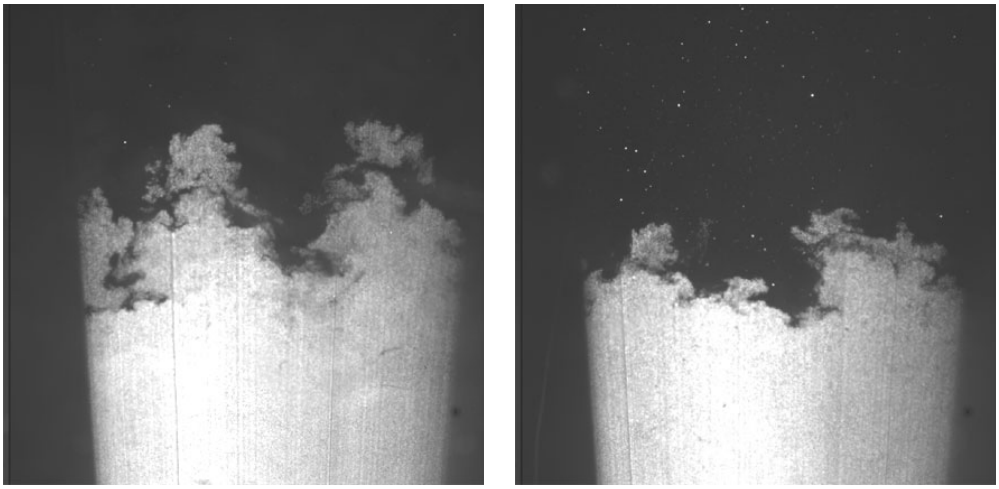

(a) (b)

Figure 11: Shocked interfaces 1.26 ms after the initial shock acceleration. Both images correspond to initial R-T interfaces approximately 110 ms old and have nominally identical experimental parameters.

the initial conditions dynamically during a R-M experiment. At present, experiments are underway and the results will be reported in a forthcoming article.

During the very late stages of the evolution, when interaction of adjacent mushrooms results in a mixing zone, the penetration depth of the unseeded gas (CO_2 in the present case) into the smoke seeded gas (air) is difficult to determine. It is explained earlier that it is difficult to differentiate between the scattering signal off the smoke particles in the mixing zone and that off the smoke particles in pure air below. A refined technique such as Rayleigh scattering, implemented with a more powerful laser than the one currently available would overcome this limitation.

7 Conclusion

A novel technique to create a membraneless, single-mode sinusoidal interface between two gases in a vertical shock tube has been developed and demonstrated. A thin copper sheet, formed into a sinusoidal shape, initially separating the two gases of interest, is retracted to form the interface. With CO_2 above air, the initial perturbations grow due to the Rayleigh-

Taylor instability, maintaining a sinusoidal profile up to approximately 120 ms after the two gases come in contact with each other. The flowfield is found to be predominantly two-dimensional and the Rayleigh-Taylor-developed interface presents a useful nonlinear initial perturbation for the Richtmyer-Meshkov experiment. The initial interface has nominally an amplitude to wavelength ratio of 0.232. The plate retraction technique is modified further to a two stage process and an R-M experiment to accelerate the R-T-developed interface by a Mach 3.08 shock wave incident in CO_2 is designed. The R-M experiments show that the interfacial perturbations invert phase upon shock interaction, as expected for a heavy/light configuration. The perturbations are found to grow rapidly (after the phase reversal) during approximately 700 μs after the initial shock interaction. The growth rate falls rapidly thereafter and the evolution is dominated by interaction of adjacent mushrooms, resulting in a mixing zone. A comparison with nonlinear theories shows a qualitative agreement, with the prediction from Sadot *et al.*[24] agreeing best with the data. A qualitative study shows that the higher the initial nonlinearity of the perturbations, for a given post-shock delay time, the smaller is the growth factor and the sooner does the growth reach saturation. It is observed that a change in the initial conditions formed at the interface results in a markedly different growth, keeping all parameters nominally identical. In order to eliminate any uncertainty, we conclude that it is necessary to capture the initial conditions dynamically, *i.e.* just before the arrival of the shock at the interface, during an experiment.

References

[1] Lord Rayleigh. Investigation of the character of the equilibrium of an incompressible heavy fluid of variable density. *Scientific Papers, V. II*, pages 200–207, 1964. Dover Pub., NY, reprinted the 1900 papers.

[2] G. Taylor. The instability of liquid surfaces when accelerated in a direction perpendicular to their planes. I. *Proc. R. Soc. London Ser. A*, 201:532–536, 1950.

[3] R. D. Richtmyer. Taylor instability in shock acceleration of compressible fluids. *Comm. on Pure and App. Math.*, 13:297–319, 1960.

[4] Ye. Ye. Meshkov. Instability of a shock wave accelerated interface between two gases. *NASA Technical Translation, NASA TT F-13,074*, 1970.

[5] L. Smarr, J. R. Wilson, R. T. Barton, and R. L. Bowers. Rayleigh-Taylor overturn in supernova core collapse. *Astrophysical J.*, 246:515–525, 1981.

[6] J. M. Stone, J. Xu, and L. G. Mundy. Formation of 'bullets' by hydrodynamical instabilities in stellar outflows. *Nature*, 377:315–317, 1995.

[7] B. Jun, T. W. Jones, and M. L. Norman. Interaction of Rayleigh-Taylor fingers and circumstellar cloudlets in young supernova remnants. *Astrophysical J.*, 468:L59–L63, 1996.

[8] D. L. Frost. Dynamics of explosive boiling of a droplet. *Phys. Fluids*, 31(9):2554–2561, 1988.

[9] M. S. Plesset. On the stability of fluid flows with spherical geometry. *J. App. Phys.*, 25(1):96–98, 1954.

[10] J. D. Lindl and W. C. Mead. Two-dimensional simulation of fluid instability in laser-fusion pellets. *Phys. Rev. Let.*, 34(20):1273–1276, 1975.

[11] J. D. Lindl, R. L. McCrory, and E. M. Campbell. Progress toward ignition and burn propagation in inertial confinement fusion. *Physics Today*, 377(9):32–40, 1992.

[12] R. L. McCrory, L. Montierth, R. L. Morse, and C. P. Verdon. Nonlinear evolution of ablation-driven Rayleigh-Taylor instability. *Phys. Rev. Let.*, 46(5):336–339, 1981.

[13] F. E. Marble, G. J. Hendricks, and E. E. Zukoski. Progress toward shock enhancement of supersonic combustion processes. *AIAA/SAE/ASME/ASEE 23rd Joint Propulsion Conference*, AIAA-87-1880, 1987.

[14] I. A. Waitz, F. E. Marble, and E. E. Zukoski. An investigation of a contoured wall injector for hypervelocity mixing augmentation. *AIAA/SAE/ASME/ASEE 27th Joint Propulsion Conference*, AIAA-91-2265, 1991.

[15] J. Grun, M. H. Emery, S. Kacenjar, C. B. Opal, E. A. McLean, S. P. Obenschain, B. H. Ripin, and A. Schmitt. Observation of the Rayleigh-Taylor instability in ablatively accelerated foils. *Phys. Rev. Let.*, 53(14):1352–1355, 1984.

[16] M. H. Emery, J. H. Gardner, and J. P. Boris. Rayleigh-Taylor and Kelvin-Helmholtz instabilities in targets accelerated by laser ablation. *Phys. Rev. Let.*, 48(10):677–683, 1982.

[17] J. Hecht, U. Alon, and D. Shvarts. Potential flow models of Rayleigh-Taylor and Richtmyer-Meshkov bubble fronts. *Phys. Fluids*, 6(12):4019–4030, 1994.

[18] Q. Zhang and S. Sohn. Nonlinear theory of unstable fluid mixing driven by shock wave. *Phys. Fluids*, 9(4):1106–1124, 1997.

[19] G. I. Barenblatt. Selfsimilar turbulence propagation from an instantaneous plane source. pages 48–60, 1983. In: Nonlinear Dynamics and turbulence, edited by G. Barenblatt, G. Ioos and D. Joseph, Pitman, Boston, 1983.

[20] K. O. Mikaelian. Turbulent mixing generated by Rayleigh-Taylor and Richtmyer-Meshkov instabilities. *Physica D 36*, pages 343–357, 1989.

[21] K. I. Read. Experimental investigation of turbulent mixing by Rayleigh-Taylor instability. *Physica 12D*, pages 45–58, 1984.

[22] U. Alon, J. Hecht, D. Mukamel, and D. Shvarts. Scale invariant mixing rates of hydrodynamically unstable interfaces. *Phys. Rev. Let.*, 72(4):2867–2870, 1994.

[23] U. Alon, J. Hecht, D. Ofer, and D. Shvarts. Power laws and similarity of Rayleigh-Taylor and Richtmyer-Meshkov mixing fronts at all density ratios. *Phys. Rev. Let.*, 74(4):534–537, 1995.

[24] O. Sadot, L. Erez, U. Alon, D. Oron, L. A. Levin, G. Erez, G. Ben-Dor, and D. Shvarts. Study of nonlinear evolution of single-mode and two-bubble interaction under richtmyer-meshkov instability. *Phys. Rev. Let.*, 80(8):1654–1657, 1998.

[25] J. D. Ramshaw. Simple model for linear and nonlinear mixing at unstable fluid interfaces with variable acceleration. *Phys. Rev. E*, 58(5):5834–5840, 1998.

[26] M. Brouillette and B. Sturtevant. Experiments on the Richtmyer-Meshkov instability: Small-scale perturbations on a plane interface. *Phys. Fluids A*, 5(4):916–930, 1993.

[27] L. Houas and I. Chemouni. Experimental investigation of Richtmyer-Meshkov instability in shock tube. *Phys. Fluids*, 8(2):614–627, 1996.

[28] G. Jourdan, L. Houas, J. F. Haas, and G. Ben-Dor. Thickness and volume measurements of a Richtmyer-Meshkov instability-induced mixing zone in a square shock tube. *J. Fluid Mech.*, 349:67–94, 1997.

[29] B. P. Puranik, J. G. Oakley, M. A. Anderson, and R. Bonazza. Experiments on the Richtmyer-Meshkov instability, I: Preparation of a membraneless interface using the Rayleigh-Taylor instability. University of Wisconsin Fusion Technology Institute, UWFDM-1171, September 2001.

[30] M. H. Anderson, B. P. Puranik, J. G. Oakley, P. W. Brooks, and R. Bonazza. Shock tube investigation of hydrodynamic issues related to inertial confinement fusion. *Shock Waves*, 10(5):377–387, 2000.

[31] W. L. Carter and I. Hasegawa. Fixation of tobacco smoke aerosols for size distribution studies. *J. Coloid and Interface Sci.*, 53(1):134, 1975.

[32] R. M. Baltrusaitis, M. L. Gittings, R. P. Weaver, R. F. Benjamin, and J. M. Budzinski. Simulation of shock-generated instabilities. *Phys. Fluids*, 8(9):2471–2483, 1996.

[33] Y. Yang, Q. Zhang, and D. H. Sharp. Small amplitude theory of Richtmyer-Meshkov instability. *Phys. Fluids*, 6(5):1856–1873, 1994.

[34] A. R. Weeks. *Fundamentals of electronic image processing.* SPIE-The international society for optical engineering, Bellingham, Washington, 1996.